A Quantitative Investigation of Entrainment and Detrainment in Numerically Simulated Convective Clouds. Part I: Model Development

Charles Cohen
Institute for Global Change Research and Education*
Huntsville, Alabama

November, 1998

corresponding author address: Charles Cohen, Global Hydrology and Climate Center, 977 Explorer Blvd, Huntsville, AL 35806
E-mail: charlie.cohen@msfc.nasa.gov

* The Institute for Global Change Research and Education is jointly operated by the Universities Space Research Association and the University of Alabama in Huntsville.

A Quantitative Investigation of Entrainment and Detrainment in Numerically Simulated Convective Clouds. Part I: Model Development

Charles Cohen
Institute for Global Change Research and Education*
Huntsville, Alabama

Abstract

A method is developed which uses numerical tracers to make accurate diagnoses of entrainment and detrainment rates and of the properties of the entrained and detrained air in numerically simulated clouds. The numerical advection scheme is modified to make it nondispersive, as required by the use of the tracers. Tests of the new method are made, and an appropriate definition of clouds is selected.

Distributions of mixing fractions in the model consistently show maximums at the end points, for nearly undilute environmental air or nearly undilute cloud air, with a uniform distribution between.

The cumulonimbus clouds simulated here entrain air that had been substantially changed by the clouds, and detrained air that is not necessarily representative of the cloud air at the same level.

---

* The Institute for Global Change Research and Education is jointly operated by the Universities Space Research Association and the University of Alabama in Huntsville.

Abstract

A method is developed which uses numerical tracers to make accurate diagnoses of entrainment and detrainment rates and of the properties of the entrained and detrained air in numerically simulated clouds. The numerical advection scheme is modified to make it nondispersive, as required by the use of the tracers. Tests of the new method are made, and an appropriate definition of clouds is selected.

Distributions of mixing fractions in the model consistently show maximums at the end points, for nearly undilute environmental air or nearly undilute cloud air, with a uniform distribution between.

The cumulonimbus clouds simulated here entrain air that had been substantially changed by the clouds, and detrained air that is not necessarily representative of the cloud air at the same level.

1. Introduction

A vertical sounding within a convective cloud differs from a moist adiabat because the environmental air is entrained into the cloud. This entrainment also causes an increase in the mass of the cloud, which may at the same time decrease by detrainment to the environment. The relationship to large-scale dynamics of entrainment and detrainment in convective clouds became clear when Yanai *et al.* (1973) showed that the effect of clouds on the environment consists largely of warming and drying by downward motion that compensates for the upward mass flux in clouds, with additional contributions by the detrained water vapor and condensate.

One-dimensional steady-state cloud models are often used when the effect of convective clouds on the large-scale environment is parameterized in numerical models or diagnosed from large-scale budgets. Early work with these cloud models treated clouds as either steady-state jets (Stommel, 1947, 1951) or bubbles (Scorer and Ludlam, 1953; Levine, 1959) or as starting plumes (Turner, 1962). All of these models include an entrainment rate that is inversely proportional to the cloud's radius, and Simpson *et al.* (1965) concluded from both photographic measurements and simulations of observed clouds that the radius is approximately constant with height. However, when these models are used, the cloud radius must be specified.

Recently, the specified entrainment and detrainment rates in one-dimensional cloud models have been replaced by specified rates of mixing of cloud air with environmental air, with the buoyancy of the resulting mixed parcels being used to determine their subsequent paths. In the model of Raymond and Blyth (1986, 1992), for example, entrainment and mixing is conceived as a random, episodic process, and each parcel moves to its level of neutral buoyancy after mixing. Emanuel (1991), accounting for the possible presence of condensate in neutrally buoyant parcels, detrained the mixed air only at levels at which further mixing with the environment will result in neutral buoyancy. Another type of buoyancy sorting model, developed by Kain and Fritsch (1990), avoids tracing the paths of individual mixed parcels, and instead entrains into a single updraft only those mixed parcels that are positively buoyant.

Although the concept of a buoyancy sorting model is supported by observations (Taylor and Baker, 1991; Blyth and Raymond, 1988) and by two-dimensional numerical simulations (Bretherton and Smolarkiewicz, 1989), the details of the model formulation need to be tested for a variety of cloud types and for different environments.

Siebesma and Cuijpers (1995) computed entrainment and detrainment rates in a large-eddy simulation of nonprecipitating shallow convective clouds, and found that the fractional entrainment and detrainment rates used in present large-scale atmospheric models are one order of magnitude too small. Using their larger rates in a one-column model, Siebesma and Holtslag (1996) produced a more realistic simulation of heat and moisture fluxes due to small cumuli. However, their method produces only bulk entrainment and detrainment rates, not a distribution of mixing fractions, and does not distinguish between air entrained from the environment and air exchanged between updraft and downdraft. In addition, it does not yield the properties of entrained and detrained air.

Lin and Arakawa (1997b) made some inferences about entrainment rates in numerically simulated cumulonimbus clouds by comparing vertical profiles of moist static energy in clouds and averaged over the domain. This method provides entrainment rates which can be used in one-dimensional cloud models because it requires the same assumption that is in the one-dimensional cloud models, *i.e.* that the entrained air has the same properties as the horizontal

average. If, however, the entrained air has a larger moist static energy than the horizontal average, this method will produce an entrainment rate that is too small. Then, a comparison of the computed entrainment rate and the actual mass flux profile will produce a detrainment rate that is too small. This may be insignificant, because the net result of entrainment and detrainment will still produce the correct mass flux in the one-dimensional cloud model. Perhaps a more serious weakness in this method arises because moist static energy does not uniquely characterize thermodynamic properties. If, for example, the entrained air has the same moist static energy as the horizontal average, but is cooler and more moist, then the mixed parcel will have more condensate. The method used in the present study independently yields the mass flux entrainment rate, the mass flux detrainment rate, and the properties of the entrained and detrained air.

Section 2 includes descriptions of the method of using passive numerical tracers and of an improved advection algorithm that is required for this study. In Section 3, the method is tested with different definitions of clouds in the numerical model, and the one that is most appropriate for simulating cumulonimbus clouds with this method is selected.

2. Methods

a. Tracers

The fractional mass flux entrainment rate is normally defined in one-dimensional steady-state cloud models as $\Delta M/(M\Delta z)$, where $M = \rho A w$ is the mass flux, A is the horizontal area of the cloud, and w is vertical velocity. For a time-dependent cloud, we must include an additional quantity which accounts for the lateral expansion of the cloud boundary. However, the simplest way to measure entrainment in a simulated cloud is to use the mass continuity equation, as it is described in Arakawa and Schubert (1974, pp. 675-676), and measure the lateral inflow of mass.

The aim of this research is to compute entrainment and detrainment rates that can be used in one-dimensional cloud models. In these models, mass flux is specified at cloud base, and changes above cloud base only by entrainment or detrainment. Therefore, in this study, air is defined as being entrained when it first meets the definition of a cloud updraft or of a cloud downdraft, whether this occurs due to mixing with existing cloud air, due to the arrival of falling precipitation, or due to adiabatic cooling that forms a new cloud above the level of the existing cloud base. Similarly, air is defined as being detrained when it first fails to comply with the definition of a cloud updraft or of a cloud downdraft, regardless of the reason. We do not make the distinction, explained by Taylor and Baker (1991), between lateral ejection of air from inside a cloud and wake shedding, in which material that was previously rising in a convective cloud is simply left behind or actually propelled downward with little lateral motion.

No attempt is made to distinguish between lateral entrainment and cloud-top entrainment; instead we compute entrainment and detrainment rates and the properties of the entrained and detrained air. As Siebesma and Cuijpers (1995) explain, entrainment at the top of a rising parcel, when averaged over the lifetime of the cloud, is mathematically equivalent to lateral entrainment.

Eight conservative tracers will be periodically initialized as follows.

$$T_l = \begin{cases} 0 & \text{in clouds} \\ \rho\,\theta_e & \text{outside of clouds} \end{cases} \qquad (1)$$

$$T_2 = \begin{cases} 0 & \text{in clouds} \\ \rho & \text{outside of clouds} \end{cases} \quad (2)$$

$$T_3 = \begin{cases} \rho\,\theta_e & \text{in cloud updrafts} \\ 0 & \text{in cloud downdrafts or outside of clouds} \end{cases} \quad (3)$$

$$T_4 = \begin{cases} \rho\, z & \text{in cloud updrafts} \\ 0 & \text{in cloud downdrafts or outside of clouds} \end{cases} \quad (4)$$

$$T_5 = \begin{cases} \rho & \text{in cloud updrafts} \\ 0 & \text{in cloud downdrafts or outside of clouds} \end{cases} \quad (5)$$

$$T_6 = \begin{cases} \rho\,\theta_e & \text{in cloud downdrafts} \\ 0 & \text{in cloud updrafts or outside of clouds} \end{cases} \quad (6)$$

$$T_7 = \begin{cases} \rho\, z & \text{in cloud downdrafts} \\ 0 & \text{in cloud updrafts or outside of clouds} \end{cases} \quad (7)$$

$$T_8 = \begin{cases} \rho & \text{in cloud downdrafts} \\ 0 & \text{in cloud updrafts or outside of clouds} \end{cases} \quad (8)$$

where θ_e is equivalent potential temperature. These definitions are designed for a numerical model with height, z, as the vertical coordinate, and with constant horizontal and vertical grid intervals, in which case density, ρ, is a measure of the mass in a grid box. They can be changed for other types of grids; if the vertical coordinate used a constant pressure interval, for example, ρ would be replaced by 1.

After a fixed interval, Δt_T, the value of T_2/ρ at a cloudy grid point is the fraction of the air in that grid box which was entrained from the environment during the interval; $1 - T_2/\rho$ is the fraction of air that was outside of the cloud at the beginning of the interval. The distribution of mixing fractions of mass is given by the values of T_2/ρ throughout the model domain, including only those grid points where $0 < T_2/\rho < 1$.

At each grid level, at the end of each Δt_T, the quantity $T_2 A$, where A is the horizontal area of the grid box, is added over all points in cloud updrafts. At the end of the simulation, this sum is divided by the duration of the simulation to give the environmental mass added to the cloud updraft per unit height and per unit time. This includes both inward horizontal mass flux and horizontal expansion of the updraft. When this sum is divided by the time-averaged updraft mass flux, we get the fractional entrainment rate of environmental air into the updraft.

The same calculation, using T_8 in place of T_2, gives the fractional entrainment rate of downdraft air into the updraft.

Similar calculations, using T_2 and T_5, produce the fractional entrainment rates of environmental air and updraft air into the downdraft.

Adding the quantity $T_5 A$ outside of the cloud updrafts, and proceeding as above, gives the fractional detrainment rate for the updraft. In the same way, the fractional detrainment rate for the downdraft uses the sum of $T_8 A$ outside of cloud downdrafts.

The θ_e of environmental air entrained into the updraft was T_1/T_2 at the start of the interval, when the tracers were initialized, before the air was entrained. The quantity T_6/T_8 is

the θ_e of downdraft air entrained into the updraft. Similar calculations are done for air entrained into the downdraft.

Evaluating T_3/T_5 outside of updrafts and T_6/T_8 outside of downdrafts gives the θ_e of detrained air.

Because θ_e changes due to freezing and melting, and due to deposition and sublimation, the tracers will accurately give the value for air entrained from the environment, but may be slightly inaccurate for detrained air or for air transferred between updraft and downdraft. This problem can be minimized by specifying the smallest interval Δt_T that gives accurate results.

The tracers T_4 and T_7 enable us to assign entrainment and detrainment to the correct levels. For example, an updraft parcel which is at a height z_f at the end of an interval has risen from the height T_4/T_5. Therefore any entrained air that is present in the parcel was entrained somewhere between $z = T_4/T_5$ and $z = z_f$. Similarly, we know that if detrained updraft air started the interval at $z = T_4/T_5$, it must have been detrained somewhere between $z = T_4/T_5$ and $z = z_f$. Interpolation is necessary when $z = T_4/T_5$ is not exactly at a model grid level.

To avoid numerical problems that would arise when very small amounts of entrained or detrained air result in very small values of the tracers, all quantities are accumulated over time at each grid level before the ratios are computed. For this reason, entrainment and detrainment rates can be computed only as averages over space and time, not as instantaneous rates at a point.

b. Advection and diffusion

If the entrainment process in numerically simulated clouds is to be used to learn about the same process in real clouds, we must be confident that entrainment and mixing in the model are simulations of real physical processes, and not due primarily to numerical diffusion.

In the RAMS model (Pielke *et al.*, 1992; Walko *et al.*, 1995), there are two independent types of mixing, the parameterized subgrid-scale turbulence, and any diffusion that might be present in the advection scheme. The subgrid-scale turbulence uses eddy diffusion coefficients which are computed, following the original formulation of Smagorinsky (1963) and Lilly (1962), as the product of the local fluid deformation rate and the square of a length scale which is related to the grid cell dimensions. Because of this dependence on the square of the length scale, the parameterized turbulent diffusion, as shown by Williamson (1978), decreases with a decreasing grid size. We can therefore minimize the subgrid-scale turbulence by using a sufficiently small grid interval. A more physical interpretation is given by Klaassen and Clark (1985), who explain that if the mesh is fine enough to resolve the eddies containing the major part of the flow's kinetic energy, then the eddy mixing terms make only a small contribution to the dynamics.

There are two advection schemes available in RAMS, forward (Tremback *et al.*, 1987) and leapfrog. The standard procedure is to apply a hybrid of the two, in which the leapfrog scheme is used for velocity components and pressure, with all other prognostic variables using the forward scheme. A third advection procedure (Stevens *et al.*, 1998), a flux-corrected transport scheme based on the work of Zalesak (1979), was written for the RAMS model. This scheme, unlike many other advection formulations, is monotonic, *i.e.* when the velocity is constant, the finite difference scheme does not generate any new maxima or minima. This is important for the present simulations, because if a passive tracer is initialized with a

discontinuity at the edge of a cloud, then a dispersive advection scheme will incorrectly generate values of the tracer that appear to indicate entrainment in the interior of the cloud, or detrainment outside of the cloud, away from the cloud edge.

Flux-corrected transport schemes use an accurate, but dispersive, high-order scheme in conjunction with a monotonic, but diffusive, low-order scheme. The two schemes are combined with an antidiffusive operator to produce a high-order monotonic scheme. We have tested the advection scheme of Stevens *et al.* (1998) in the RAMS model and found that the diffusion decreases with a decreasing wind speed and with an increasing ratio of wavelength to grid interval. Diffusion can therefore be minimized by subtracting the vertically averaged wind in the cloud layer from the initial wind at each level. This will decrease the wind speed without changing the simulated circulation. A sufficiently small grid interval will also help to decrease the numerical diffusion in the advection scheme. Nevertheless, the diffusion in this scheme may be significant in some situations.

The forward advection scheme is applied to the moisture and thermodynamic variables and to the passive scalars when the hybrid procedure is used in the RAMS model. In contrast to the flux-corrected transport scheme, the forward scheme is dispersive but not diffusive. If the dispersive property can be removed from this scheme, it would then have the advantage over the flux-corrected transport scheme of being less diffusive.

Rood (1987, p. 83) describes a few varieties of filling procedures, in which negative values of positive-definite quantities are set to zero, with values at other points adjusted in order to maintain a constant average over the domain. Although these procedures are effective in removing negative values, they do not entirely remove new maxima or minima that are generated by the advection scheme. Therefore, we have implemented a procedure in which new maxima or minima are removed after the RAMS forward scheme is applied. The idea is that advection should not, by itself, increase a maximum or decrease a minimum. Separately for each direction[1], if the new value of a prognostic variable at a point is larger than the maximum of the old values at that point and at the two immediately surrounding points, then the new value is reduced to the old maximum. The values at the two surrounding points are then increased, in proportion to how close they already are to the maximum. A similar procedure is applied when the new value is smaller than the minimum of the old values. Finally, the domain-average is corrected by a multiplicative adjustment. This technique may be viewed as a generalization of the one described by Rasch and Williamson (1990, p. 1076); it differs from the procedure of Bermejo and Staniforth (1992) in the adjustment to the two surrounding points.

Fig. 1 shows the results of a comparison of preliminary tests of the advection schemes. These one-dimensional simulations advect a passive tracer, with $u\Delta t / \Delta x = 0.5$, for 100 time steps, as in Figs 1, 2, and 5 of Rood (1987). For the square wave, the forward-in-time scheme produces non-physical values less than zero and greater than one. These are eliminated with the flux-corrected transport scheme, but a significant diffusion is added. (As stated above, this diffusion can be partly eliminated in simulations of clouds.) The new scheme comes close to preserving the shape of the square wave without introducing any new maxima or minima. For the triangular wave, although the new procedure eliminates the very small negative values, it is not much of an improvement. It slightly reduces the maximum, because the new procedure

[1] The forward advection scheme in RAMS uses the splitting or Marchuk method (Mesinger and Arakawa, 1976), in which the advected variable is updated after the advection is performed for each direction.

changes the maximum only when the RAMS forward advection scheme has increased it, not when it has decreased it.

c. model description

The compressible nonhydrostatic option of the RAMS model is used in this study. The model is run in two dimensions, with a domain 500 km wide and 19 km in height, with grid intervals 1000 m in the horizontal and 300 m in the vertical. A rigid lid is invoked at the model top by constraining vertical velocity to be zero there. Lateral boundary conditions are formulated as in Klemp and Wilhelmson (1978). Open lateral boundaries are possible in the present simulations because there are no simulated clouds near the edges of the domain. If a cloud were to be advected out of the domain, the tracers would not correctly diagnose the entrainment and detrainment rates.

Surface heat and moisture fluxes and radiation are not included in the present simulations.

The prognostic variables are ice-liquid water potential temperature (Tripoli and Cotton, 1981) and mixing ratios of rain, pristine ice crystals, snow, aggregates, graupel, hail, and total water substance. Temperature, water vapor mixing ratio, and cloud water mixing ratio are diagnosed (Tripoli and Cotton, 1982).

The initial sounding, shown in Fig. 2, was formulated in order to simulate deep convection that is similar to what might be observed over a midlatitude continent in the summer.

The aim of the present study is to examine the entrainment and detrainment processes in clouds that are produced by the initial sounding. We do not want to simulate clouds generated by an environment that has been significantly changed by the convection. Therefore the initial state is designed to quickly generate deep convection that lasts for only a limited period of time. To accomplish this, convection is initiated with two 2-km-deep semi-infinite cold pools, each with a maximum potential temperature deficit at the surface of -8 K, decreasing linearly to zero at 2 km. The cold pools surround a 50-km-wide region of undisturbed air in the center of the domain. Shortly after one hour, the cold pools converge, suddenly eliminating the supply of conditionally unstable air to the convection, resulting in a simulation of the complete life cycle of convection generated by the initial sounding.

The initial wind increases from -10 m s^{-1} at the surface to 5 m s^{-1} at 2.5 km, and is constant with height above that. Consistent with the results of Thorpe et al. (1980), the much stronger initial cloud generated by the eastward-moving cold pool completely dominates the simulation. A constant is subtracted from the wind at each level in order to keep the clouds approximately stationary near the center of the domain.

The same simulation is interpreted using three definitions of clouds. In definition 1, cloud updrafts are defined by $w > 0$ and $q_c + q_i > 0.01$ g kg^{-1}, where q_c and q_i are the mixing ratios of cloud water and pristine ice crystals, while cloud downdrafts are defined by $w < 0$ and total condensate > 0.01 g kg^{-1}. In definition 2, the updrafts must only have total condensate > 0.01 g kg^{-1}, while definition 3 is the same as definition 1 except that a cloud must have $|w| > 0.5$ m s^{-1}.

3. Results

a. distribution of mixing fractions

The distribution of mixing fractions using definition 3 is shown in Fig. 3. In order to exclude grid points with only negligible degrees of mixing, the frequency distribution includes only those points with $0.01 < T_2/\rho < 0.99$. The distribution does not vary with height within the cloud (not shown). Distributions with the same shape have been produced for other simulations (not shown) of a variety of convective cloud types, using a range of grid intervals from 2.5 m to 2000 m.

With the 1000 m horizontal grid of the present study, entrainment is almost entirely a result of turbulent diffusion at the edges of clouds. However, simulations by Klaassen and Clark (1985), Grabowski (1989), and Grabowski and Clark (1991, 1993) of small cumulus clouds with a very fine resolution have revealed an additional entrainment process. This is an inviscid process associated with the baroclinic production of vorticity due to horizontal buoyancy gradients across the cloud-environment interface. The fact that the distribution of mixing fractions does not vary with grid size suggests that no significant quantitative error is made in simulating entrainment with a coarse grid, which substitutes parameterized subgrid-scale turbulence for the inviscid baroclinic process.

Although the present results resemble the uniform distribution used by Raymond and Blyth (1986, 1992) and Emanuel (1991) much more than they resemble the normal distribution used by Kain and Fritsch (1990), the conceptual model used here, of air being entrained into an existing cloud, is the same as that of Kain and Fritsch. Compared to a normal distribution of mixing fractions, the distribution of Fig. 3 would result in a larger fraction of the entrained air coming from nearly pure environmental air, and a larger fraction of the detrained air coming from nearly undilute cloud air. Compared to a uniform distribution, the same would be true, but to a much lesser extent. Whether this has a significant impact on the results of buoyancy sorting models needs to be determined.

b. entrainment and detrainment for different definitions of clouds

Deep convection dissipates before three hours, but the simulations were run for 10 h in order to be sure that the clouds would have time to dissipate by the end of each simulation. This guarantees that the time-averaged time tendencies are zero, and that the entrainment and detrainment rates can therefore be interpreted as vertical gradients of mass flux. (See Eqs. 3 and 4 of Arakawa and Schubert, 1974.) With the third definition of clouds, shorter simulations would have been just as good.

To verify that the tracers give accurate results, the quantity $\Delta M/(M\Delta z)$ was computed at each grid level, for the updrafts and the downdrafts, using the diagnosed entrainment and detrainment rates, and compared to the actual value (Figs. 4a and 4c). In addition, the vertical gradient of θ_e was computed, for the updrafts and downdrafts, using the diagnosed entrainment and detrainment rates and the diagnosed θ_e in the entrained and detrained air, and compared to the actual vertical gradient (Figs. 4b and 4d). As shown in Fig. 4, the diagnostic procedure described in section 2a is sufficiently accurate to enable us to draw general conclusions about entrainment and detrainment. Freezing and deposition may partially explain why θ_e in the updraft increases with height in the upper troposphere faster than is diagnosed by the tracers (Fig. 4b). At the top of the cloud, where mass flux is small and therefore fractional entrainment and detrainment rates are large, the results are generally not useful. The reconstruction of the fractional change of downdraft mass flux with height (Fig. 4c) is more accurate for the smaller

interval, Δt_T = 100 sec. In general, results are slightly more accurate using the 100 sec. interval, but the results do not continue to improve as the interval is reduced towards one time step.

The time- and space-averaged entrainment and detrainment rates for definition 1 are shown in Fig. 5. Because, in the design of the tracers, no distinction is made between air below or above clouds and air alongside of clouds, air feeding the cloud from below cloud base appears as a large entrainment rate in a thin layer near cloud base, and detrainment at the ultimate cloud top appears as a large detrainment rate in a thin layer near cloud top. Between these two thin layers are found the lateral entrainment and detrainment rates, which are the more interesting results.

Because the results are averaged over time and space, the net change in mass flux with height is a relatively small difference between larger entrainment rates and detrainment rates. This is consistent with the observations of real clouds by Barnes et al. (1996) who diagnosed net entrainment and later net detrainment in the same layer, and by Perry and Hobbs (1996), who inferred that cumulus clouds grow on the upshear side and decay on the downshear side. As we will see, however, the magnitudes of the entrainment and detrainment rates depend on the definition of clouds in the numerical model.

Through nearly the entire depth of the cloud, if we look at the net result of entrainment and detrainment, we see that the updraft (Fig. 5a) is gaining air from the environment and losing air to the downdraft. There appears to be an excessively large rate of exchange of air between the updraft and the downdraft above 9 km, but, as shown in Fig. 6b, at these levels, the updraft, the downdraft, and the air transferred between the two have almost identical values of θ_e. This represents small-scale oscillations in a persistent but very small cirrus anvil, in an environment with small horizontal gradients of θ_e. Nevertheless, the time-averaged updraft mass flux (Fig. 7) decreases with height above 10 km due to transfer of air to the downdraft, not to the environment, *i.e.* the updraft is losing its upward motion, not its pristine ice crystals.

This transfer of cloud mass flux above 10 km from updraft to downdraft using definition 1 is also evident in Fig. 5b. Below about 9 km, where the downdraft exchanges a large amount of mass flux with the environment, the downdraft is generally gaining mass flux from the updraft and losing it to the environment.

In contrast to the assumptions that are made in designing 1D cloud models, entrained and detrained air generally have similar values of θ_e (Fig. 6). The updraft is entraining air from an environment that it has modified, and is detraining air with a lower θ_e than the average for the updraft.

If, instead of defining the updraft by $q_c + q_i > 0.01$ g kg^{-1}, it must only have total condensate at least 0.01 g kg^{-1} (definition 2), then there is more updraft mass flux below 12 km (Fig 7a). In addition, in the middle troposphere, there is a much larger exchange of air between updraft and downdraft (Fig. 8a vs. Fig.5a) and the horizontally averaged θ_e of the updraft is significantly lower (Fig. 9a vs. Fig.6a). The extra updraft mass flux in the PBL using definition 2 (Fig. 7) is coming largely from the downdraft, not from the environment; it is cold air that is rising behind the gust front. In the middle troposphere with definition 2, the updraft and the downdraft have similar values of θ_e (Fig. 9b). The most obvious change from definition 1 at this height is that the downdraft is exchanging air mostly with the updraft, not with the environment (Fig. 8b vs. Fig.5b). This is due to a large amount of unsaturated rising air, with

low θ_e, with precipitation but without cloud water or pristine crystals, that is classified as environment with definition 1, but is part of the updraft with definition 2.

As with definition 1, the updraft below 5 km using definition 2 is entraining and detraining air with very similar θ_e (Fig. 9a). In contrast to definition 1, however, the air entrained from the environment to the updraft above 6 km with definition 2 has a θ_e nearly the same as that of the environment. This entrained air is forming the unsaturated parts of the updraft. With all this unsaturated air included in the updraft, the updraft θ_e is much lower, very close to that of the downdraft (Fig. 9b).

Much of the cloud mass flux which was diagnosed in the upper troposphere using the first two definitions should be classified as cirrus anvil, not as cumulonimbus cloud. By requiring that a cloud must have $|w| > 0.5$ m s^{-1} (definition 3) this air can be eliminated from the definition of a cloud. With this definition, there is less updraft mass flux above 7 km, and between about 1.5 km and 4 km (Fig. 7). The decrease in downdraft mass flux extends through the depth of the troposphere, due to weak, mostly unsaturated, downdrafts that exist during and after the period when the cumulonimbus clouds are dissipating.

When clouds are defined with $|w| > 0.5$ m s^{-1}, the large rate of exchange of air between the updraft and the downdraft above 9 km is eliminated (Fig. 10). With the updraft and the downdraft both entraining air largely from the environment and detraining air mostly to the environment, the third definition of clouds produces entrainment and detrainment rates that resemble those in traditional conceptual models. This results, however, simply because an air parcel must change its vertical velocity by ± 1 m s^{-1} within the interval Δt_T in order to transfer between updraft and downdraft. Consequently, for the larger interval, there is more exchange of air between updraft and downdraft and less between updraft and environment.

Fig. 11 shows the average properties of the entrained and detrained air for the updrafts using definition 3, combining air exchanged either with the environment or with the downdraft. The results are qualitatively similar for all three intervals. The low values of θ_e near cloud base are most likely due to air which is not rising to high levels in the updraft. Between 2 km and 4 km, θ_e of entrained air is very close to halfway between θ_e of the environment and of the updraft. This is consistent with the modeling results of Alfonso *et al.* (1998), who found that their 1D simulations most closely resembled the observations when the cloud entrained air with a water vapor mixing ratio of an equal mixture of cloud and environmental air. Just above the environmental θ_e minimum, from 5 km to 7 km, the updraft entrains air with a θ_e about 6 K higher than the environment. Above 7 km, where the time-averaged updraft mass flux is decreasing with height, the updraft θ_e increases with height more slowly than that of the environment. Entrained air at this level has a higher θ_e than detrained air, even though the environment has a lower θ_e than the updraft. As the updraft loses mass flux with increasing height in the upper part of the cloud, its θ_e increases, remaining higher than that of the environment, not only due to freezing (which occurs up to 10 km) and deposition, but also because part of the updraft with relatively low θ_e is being detrained. With only the high-θ_e air remaining, the distribution of updraft θ_e around the mean at each level is narrower above 7 km (Fig. 12).

In their 2D simulations of maritime tropical convection, Lin and Arakawa (1997b) found that the moist static energy in cloud updrafts at cloud base was about 2 kJ kg^{-1} higher than the

domain average at the surface. Fig. 11, in contrast, compares θ_e in clouds to the undisturbed initial sounding. In the present simulations, with the clouds initiated by semi-infinite cold pools, the domain average of θ_e near the surface would be determined mostly by the specified cold pools. When clouds are initiated by small random temperature perturbations, as in Lin and Arakawa (1997b), the domain average is similar to a grid-volume average in a coarse-grid model. A comparison of θ_e in the updraft and in the undisturbed environment in the present simulations is more applicable to a situation where a 1D cloud model is initialized with an observed sounding. We see that the updraft is not derived from undilute surface air.

Horizontal and temporal variations of θ_e in the updrafts provide one explanation for the low average θ_e of the updraft compared to the θ_e of the surface air in the initial undisturbed sounding. At 40 minutes (Fig. 13a), when the cloud is growing, θ_e at 5 km is as much as 350.5 K where the mass flux is strongest, but is as low as 340 K just 2 km to the east. The maximum θ_e below cloud base at this time is 356 K. Forty minutes later (Fig. 13b), just after the cold pools have converged, when the convection is much weaker, the sub-cloud air has a lower θ_e, and in the updraft at 5 km, θ_e varies from 334 K to 342 K. Cloud properties diagnosed here represent averages over space and time, over the complete life cycle of the clouds.

Lin and Arakawa (1997b) inferred that the entrainment rates just above cloud base in their simulated updrafts were larger than they were further aloft. Fig. 14, showing the total entrainment and detrainment rates, *i.e.* for air exchanged either with the environment or with the downdraft, verify this. Fractional entrainment and detrainment rates are both very small in the mid-troposphere, just above the environmental θ_e minimum, and larger near cloud base and cloud top.

Wang and Prinn (1998), in simulations of the transport of a chemical tracer in cumulonimbus clouds, similarly noted that the domain-average mole fraction of the tracer was smallest between 6 km and 9 km in height, and then inferred that the transport was primarily vertical below 9 km and switched to horizontal above that level.

The entrainment and detrainment rates for the updrafts using definition 3 (Fig. 14) are smaller when they are diagnosed using a larger interval, Δt_T, because the larger interval eliminates the small-scale, short-period, exchange of air between cloud and environment. If we compare the average θ_e of the entrained and detrained air (Fig. 11), we see that there is a larger difference between the properties of the entrained air and of the detrained air for the larger interval. This is consistent with the assumption that some air is rapidly exchanged between updraft and environment without changing its θ_e significantly. Michaud (1998) decided that since this air would have little effect on the updraft properties, it can be ignored in designing a 1D cloud model. Using the longer interval may therefore come closer to diagnosing an exchange of air between the cloud and the undisturbed environment. However, even with the longer interval, the updraft is entraining air with a higher θ_e than the undisturbed environment, and detraining air that is generally different from the average updraft air.

Between 2 km and 4 km, where the entrainment rates are relatively large (Fig. 14), and entrained air has a lower θ_e than detrained air (Fig. 11), the θ_e of the entrained air is nearly identical for the three intervals, but air with a higher θ_e is detrained for a larger interval. At this level, apparently, the air that is quickly exchanged between updraft and environment has the

same θ_e as the entrained air. Above 7 km, where mass flux is decreasing with height (Fig. 7), both entrained and detrained air have different θ_e for different intervals.

For the downdraft using definition 3, the average θ_e for entrained and detrained air is shown, in Fig. 15, only for a 100 sec. interval, because the results for the other intervals are nearly indistinguishable. Above 4 km, the downdraft θ_e is only a few degrees higher than that of the environment. As the downdraft descends to just above the environmental θ_e minimum, it detrains air with a θ_e that is slightly, but consistently, higher than the average for the downdraft. At the same time, entrained air also causes a slow steady decrease in the average θ_e of the downdraft. From 4 km to 2 km, the situation reverses, as the entrained air has a higher θ_e than the detrained air.

Through a large part of the depth of the clouds, especially in the middle troposphere, the entrainment and detrainment rates are much larger for the downdraft than they are for the updraft (Fig. 10). Consistent with this, the downdraft θ_e (Fig. 15) is closer to that of the environment than is the updraft θ_e (Fig. 11). This supports the results of Lin and Arakawa (1997a), who found, in their numerical simulation of maritime tropical cumulonimbus clouds, that no cloud air parcel descended more than several hundred meters.

4. Conclusions

A method has been developed which uses numerical tracers to make accurate diagnoses of entrainment and detrainment rates and of the properties of the entrained and detrained air in numerically simulated clouds. To obtain useful results, a nondispersive advection scheme is required, and an appropriate definition of clouds must be selected.

Because including $|w| > 0.5$ m s^{-1} in the definition of a cloud excludes the cirrus anvil, and because defining an updraft by a minimum of cloud water and pristine crystals instead of by a minimum of total condensate eliminates the unsaturated parts of the updraft, the simulations described in Part II (Cohen, 1998) will use the third definition of clouds.

This definition was shown to be suitable for simulations of deep cumulonimbus clouds; other cloud types may require different definitions.

Others (*e.g.* Xu, 1995) have devised methods of distinguishing convective clouds from stratiform clouds in numerical models. An additional consideration, disclosed here, is the presence, at the edge of convective clouds, of unsaturated ascending air that contains precipitation. This air, which is not classified as a convective cloud according to the definition selected here, and is certainly not stratiform cloud, would significantly decrease the horizontally averaged θ_e of the updraft if it were categorized as convective cloud, as it would be in many definitions currently in use.

The cumulonimbus clouds simulated here entrained air that had been substantially changed by the clouds, and detrained air that was not necessarily representative of the cloud air at the same level. Therefore, a given amount of entrainment may not change the properties of the cloud by as much as it would if air from the undisturbed environment had been entrained, and detrainment can have a significant effect on the thermodynamic properties of the cloud. In the upper part of the cloud, for example, the updraft mass flux decreases with height because the low-θ_e is being detrained, leaving only the relatively undilute core at high levels.

Distributions of mixing fractions in the model consistently show maximums at the end points, for nearly undilute environmental air or nearly undilute cloud air, with a uniform distribution between. The large quantity of air that shows only a small degree of mixing between cloud and environment appears as almost pure environmental air that joins the updraft above cloud base, or as cloud air that is detrained with only a small amount of mixing.

Acknowledgments

This work was done under NASA cooperative agreement #NCC8-142.

References

Alfonso, L., D. Martinez, and C.A. Perez, 1998: Numerical simulations of tropical convective clouds over cuba using a one-dimensional and time-dependent cloud model. *Atmos. Res.*, **47-48**, 343-354.

Arakawa, A., and W.H. Schubert, 1974: Interaction of a cumulus cloud ensemble with the large-scale environment, Part I. *J. Atmos. Sci.*, **31**, 674-701.

Barnes, G.M., J.C. Fankhauser, and W.D. Browning, 1996: Evolution of the vertical mass flux and diagnosed net lateral mixing in isolated convective clouds. *Mon. Wea. Rev.*, **124**, 2764-2784.

Bermejo, R., and A. Staniforth, 1992: The conversion of semi-Lagrangian advection schemes to quasi-monotone schemes. *Mon. Wea. Rev.*, **120**, 2622-2632.

Blyth, A. M., and D.J. Raymond, 1988: Comparisons between observations of entrainment in Montana cumuli and results from a simple model. *J. Atmos. Sci.*, **45**, 1965-1969.

Bretherton, C.S., and P.K. Smolarkiewicz, 1989: Gravity waves, compensating subsidence and detrainment around cumulus clouds. *J. Atmos. Sci.*, **46**, 740-759.

Cohen, C., 1998: A quantitative investigation of entrainment and detrainment in numerically simulated convective clouds. Part II: Simulations of cumulonimbus clouds. *J. Atmos. Sci.*, submitted.

Emanuel, K.A., 1991: A scheme for representing cumulus convection in large-scale models. *J. Atmos. Sci.*, **48**, 2313-2335.

Grabowski, W.W., 1989: Numerical experiments on the dynamics of the cloud-environment interface: small cumulus in a shear-free environment. *J. Atmos. Sci.*, **46**, 3513-3541.

------ and T.L. Clark, 1991: Cloud-environment interface instability: rising thermal calculations in two spatial dimensions. *J. Atmos. Sci.*, **48**, 527-546.

------ and ------, 1993: Cloud-environment interface instability. Part II: Extension to three spatial dimensions. *J. Atmos. Sci.*, **50**, 555-573.

Kain, J.S., and J.M. Fritsch, 1990: A one-dimensional entraining/detraining plume model and its application in convective parameterization. *J. Atmos. Sci.*, **47**, 2784-2802.

Klaassen, G.P., and T.L. Clark, 1985: Dynamics of the cloud-environment interface and entrainment in small cumuli: two-dimensional simulations in the absence of ambient shear. *J. Atmos. Sci.*, **42**, 2621-2642.

Klemp, J.B., and R.B. Wilhelmson, 1978: The simulation of three-dimensional convective storm dynamics. *J. Atmos. Sci.*, **35**, 1070-1096.

Levine, J., 1959: Spherical vortex theory of bubble-like motion in cumulus clouds. *J. Meteor.*, **16**, 653-662.

Lilly, D.K., 1962: On the numerical simulation of buoyant convection. *Tellus*, **14**, 148-172.

Lin, C., and A. Arakawa, 1997a: The macroscopic entrainment processes of simulated cumulus ensemble. Part I: Entrainment sources. *J. Atmos. Sci.*, **54**, 1027-1043

------ and ------, 1997b: The macroscopic entrainment processes of simulated cumulus ensemble Part II: Testing the entrainment plume model. *J. Atmos. Sci.*, **54**, 1044-1053.

Mesinger, F., and A. Arakawa, 1976: Numerical methods used in atmospheric models. *GARP Publ. Ser. No. 17*, WMO-ICSU Joint Organizing Committee, 64 pp.

Michaud, L.M., 1998: Entrainment and detrainment required to explain updraft properties and work dissipation. *Tellus*, **50A**, 283-301.

Perry, K.D., and P.V. Hobbs, 1996: Influences of isolated cumulus clouds on the humidity of their surroundings. *J. Atmos. Sci.*, **53**, 159-174.

Pielke, R.A., W.R. Cotton, R.L. Walko, C.J. Tremback, W.A. Lyons, L.D. Grasso, M.E. Nicholls, M.D. Moran, D.A. Wesley, T.J. Lee, and J.H. Copeland, 1992: A Comprehensive Meteorological Modeling System - RAMS. *Meteor. Atmos. Phys.*, **49**, 69-91.

Rasch, P.J., and D.L. Williamson, 1990: Computational aspects of moisture transport in global models of the atmosphere. *Quart. J. Roy. Meteor. Soc.*, **116**, 1071-1090.

Raymond, D.J., and A.M. Blyth, 1986: A stochastic mixing model for nonprecipitating cumulus clouds. *J. Atmos. Sci.*, **43**, 2708-2718.

------ and ------, 1992: Extension of the stochastic mixing model to cumulonimbus clouds. *J. Atmos. Sci.*, **49**, 1968-1983.

Rood, R.B., 1987: Numerical advection algorithms and their role in atmospheric transport and chemistry models. *Rev. Geophys.*, **25**, 71-100.

Scorer, R.S., and F.H. Ludlam, 1953: Bubble theory of penetrative convection. *Quart. J. Roy. Meteor. Soc.*, **79**, 94-103.

Siebesma, A.P., and J.W.M. Cuijpers, 1995: Evaluation of parametric assumptions for shallow cumulus convection *J. Atmos. Sci.*, **52**, 650-666.

------ and A.A.M. Holtslag, 1996: Model impacts of entrainment and detrainment rates in shallow cumulus convection. *J. Atmos. Sci.*, **53**, 2354-2364.

Simpson, J., R.H. Simpson, D.A. Andrews, and M.A. Eaton, 1965: Experimental cumulus dynamics. *Rev. Geophys.*, **3**, 387-431.

Smagorinsky, J., 1963: General circulation experiments with the primitive equations. I. The basic experiment. *Mon. Wea. Rev.*, **116**, 1927-1944.

Stevens, B., C-H Moeng, and P. P. Sullivan, 1998: Subgrid sensitivities in large-eddy simulations of radiatively driven convection. *J. Atmos. Sci.*, submitted.

Stommel, H., 1947: Entrainment of air into a cumulus cloud. *J. Meteor.*, **4**, 91-94.

------, 1951: Entrainment of air into a cumulus cloud II. *J. Meteor.*, **8**, 127-129.

Taylor, G.R., and M.B. Baker, 1991: Entrainment and detrainment in cumulus clouds. *J. Atmos. Sci.*, **48**, 112-121.

Thorpe, A.J., M.J. Miller, and M.W. Moncrieff, 1980: Dynamical models of two-dimensional downdraughts. *Quart. J. Roy. Meteor. Soc.*, **106**, 463-484.

Tremback, C.J., J. Powell, W.R. Cotton, and R.A. Pielke, 1987: The forward-in-time upstream advection scheme: extension to higher orders. *Mon. Wea. Rev.*, **115**, 540-555.

Tripoli, G.J., and W.R. Cotton, 1981: The use of ice-liquid water potential temperature as a thermodynamic variable in deep atmospheric models. *Mon. Wea. Rev.*, **109**, 1094-1102.

------ and ------, 1982: The Colorado State University three-dimensional cloud / mesoscale model - 1982. Part I: General theoretical framework and sensitivity experiments. *J. Rech. Atmos.*, **16**, 185-219.

Turner, J.S., 1962: The 'starting plume' in neutral surroundings. *J. Fluid. Mech.*, **13**, 356-368.

Walko, R.L., W.R. Cotton, M.P. Meyers, and J.Y. Harrington, 1995: New RAMS cloud microphysics parameterization. Part I: the single-moment scheme. *Atmos. Res.*, **38**, 29-62.

Wang, C., and R.G. Prinn, 1998: Impact of the horizontal wind profile on the convective transport of chemical species. *J. Geophys. Res.*, **103**, 22063-22071.

Williamson, D.L., 1978: The relative importance of resolution, accuracy and diffusion in short-range forecasts with the NCAR global circulation model. *Mon. Wea. Rev.*, **106**, 69-88.

Xu, K.-M., 1995: Partitioning mass, heat, and moisture budgets of explicitly simulated cumulus ensembles into convective and stratiform components. *J. Atmos. Sci.*, **52**, 551-573.

Yanai, M., S. Esbensen, and J.-H. Chu, 1973: Determination of bulk properties of tropical cloud clusters from large-scale heat and moisture budgets. *J. Atmos. Sci.*, **30**, 611-627.

Zalesak, S.T., 1979: Fully multidimensional flux-corrected transport algorithms for fluids. *J. Comput. Phys.*, **31**, 335-362.

Figure captions

Fig. 1: Advection of rectangle (left) and triangle (right) using the RAMS forward-in-time scheme (top), flux-corrected transport (middle), and the RAMS forward-in-time scheme with fixer (bottom). The final state (dashed) is superimposed on the initial state (solid).

Fig. 2: Initial temperature and dewpoint sounding.

Fig. 3: Distribution of mixing fractions for definition 3 using intervals of 100 sec. (solid), 200 sec. (dashed), and 300 sec. (dotted) between re-initializing the tracers.

Fig. 4: Fractional change of mass flux with height for the updraft (a) and downdraft (c), and vertical gradients of equivalent potential temperature in the updraft (b) and downdraft (d), using definition 3. The heavy solid lines show the actual values in the simulation; the thin lines show the values computed from the quantities diagnosed with the tracers, using intervals of 100 sec. (solid), 200 sec. (dashed), and 300 sec. (dotted).

Fig. 5: Fractional entrainment and detrainment rates using definition 1: (a) entrainment of environmental air (solid) and downdraft air (dashed) into the updraft; detrainment of updraft air to the environment (dot-dash) and to the downdraft (dotted); (b) entrainment of environmental air (solid) and updraft air (dashed) into the downdraft; detrainment of downdraft air to the environment (dot-dash) and to the updraft (dotted).

Fig. 6: Equivalent potential temperature: (a) undisturbed initial sounding (solid), updraft (dashed), and, using definition 1, entrained by the updraft from the environment (dot-dash) and detrained by the updraft to the environment (dotted); (b) updraft (solid), downdraft (dashed), and, using definition 1, transferred from updraft to downdraft (dotted) and transferred from downdraft to updraft (dot-dash).

Fig. 7: Horizontally averaged, time-averaged cloud mass flux using definition 1 (dotted), definition 2 (dashed), and definition 3 (solid). Updraft mass fluxes are shown by the positive curves; downdraft mass fluxes are shown by the negative curves. Downdraft mass fluxes are identical for the first two definitions.

Fig. 8: Same as Fig. 5, but using definition 2.

Fig. 9: Same as Fig. 6, but using definition 2.

Fig. 10: Same as Fig. 5, but using definition 3.

Fig. 11: Equivalent potential temperature: undisturbed initial sounding (solid), updraft (dashed), and, for definition 3, entrained by the updraft (dot-dash) and detrained by the updraft (dotted), using intervals of (a) 100 sec., (b) 200 sec., and (c) 300 sec. between re-initializing the tracers.

Fig. 12: Probability density function of deviations of updraft θ_e from its mean value for updrafts at the same level, using definition 3, for all grid points below (solid) and above (dashed) 6.9 km.

Fig. 13: Instantaneous fields at 40 min. (top) and 80 min. (bottom) of equivalent potential temperature (solid contours, with 4 K interval) and updraft mass flux (shading). Updraft mass fluxes are shown with intervals of 5 kg m^{-2} s^{-1} (top) and 2 kg m^{-2} s^{-1} (bottom).

Fig. 14: Fractional entrainment rates (a) and fractional detrainment rates (b) for definition 3, using intervals of 100 sec. (solid), 200 sec. (dashed), and 300 sec. (dotted) between re-initializing the tracers.

Fig. 15: Equivalent potential temperature: undisturbed initial sounding (solid), downdraft (dashed), and, for definition 3, entrained by the downdraft (dot-dash) and detrained by the downdraft (dotted), using an interval of 100 sec. between re-initializing the tracers.

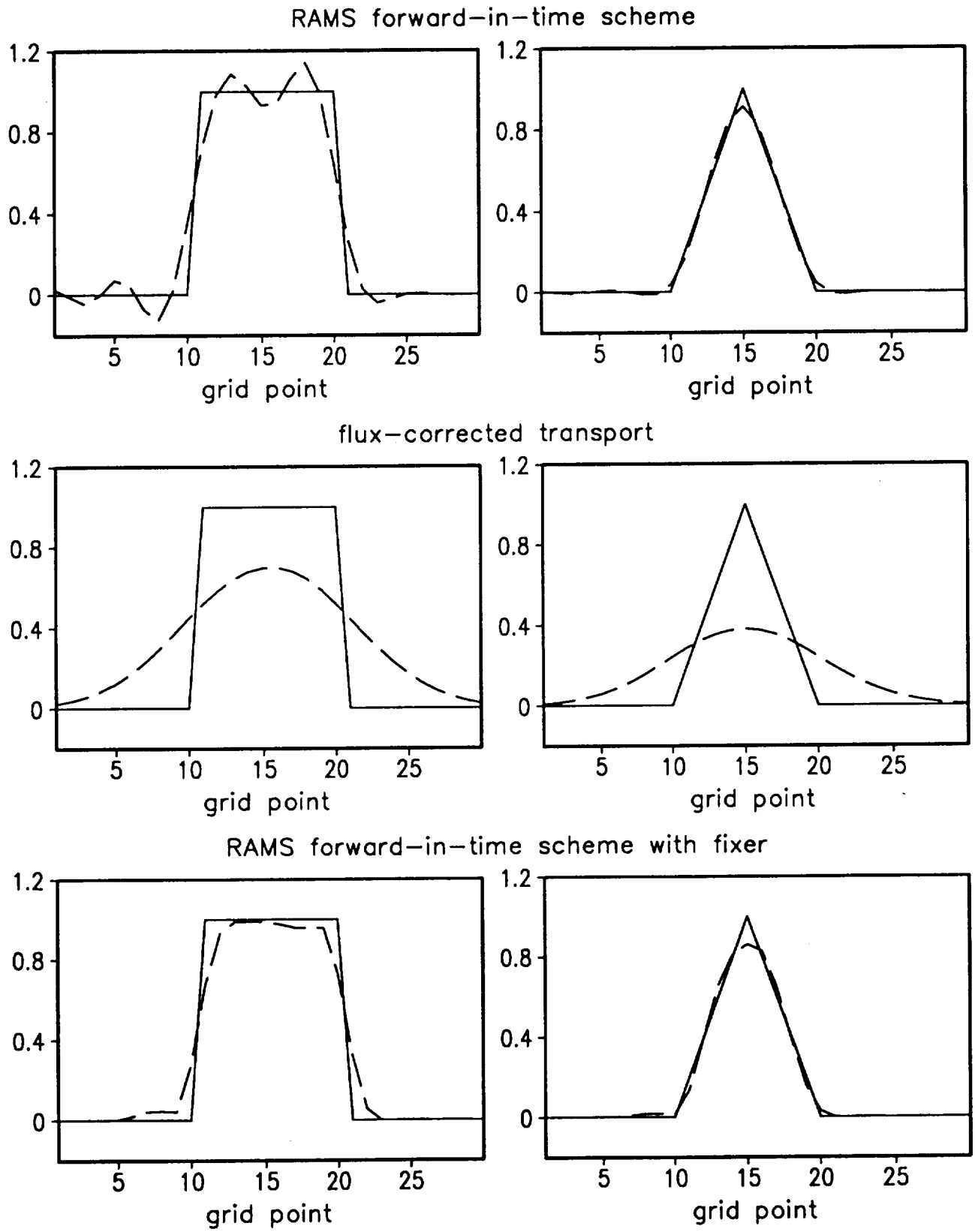

Fig. 1: Advection of rectangle (left) and triangle (right) using the RAMS forward–in–time scheme (top), flux–corrected transport (middle), and the forward–in–time scheme with fixer (bottom). The final state (dashed) is superimposed on the initial state (solid).

GrADS: COLA/IGES

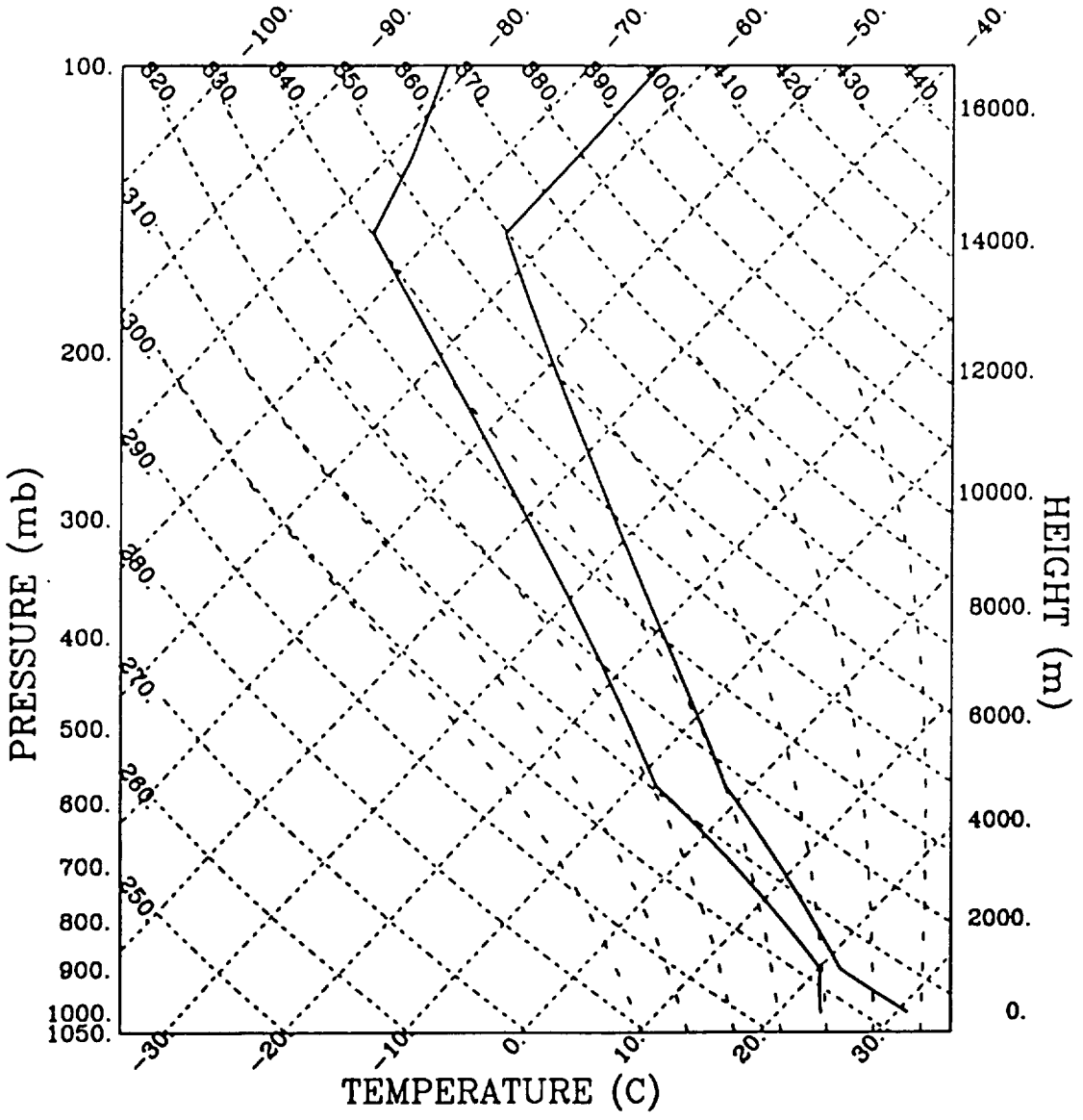

Fig. 2: Initial temperature and dewpoint soundings.

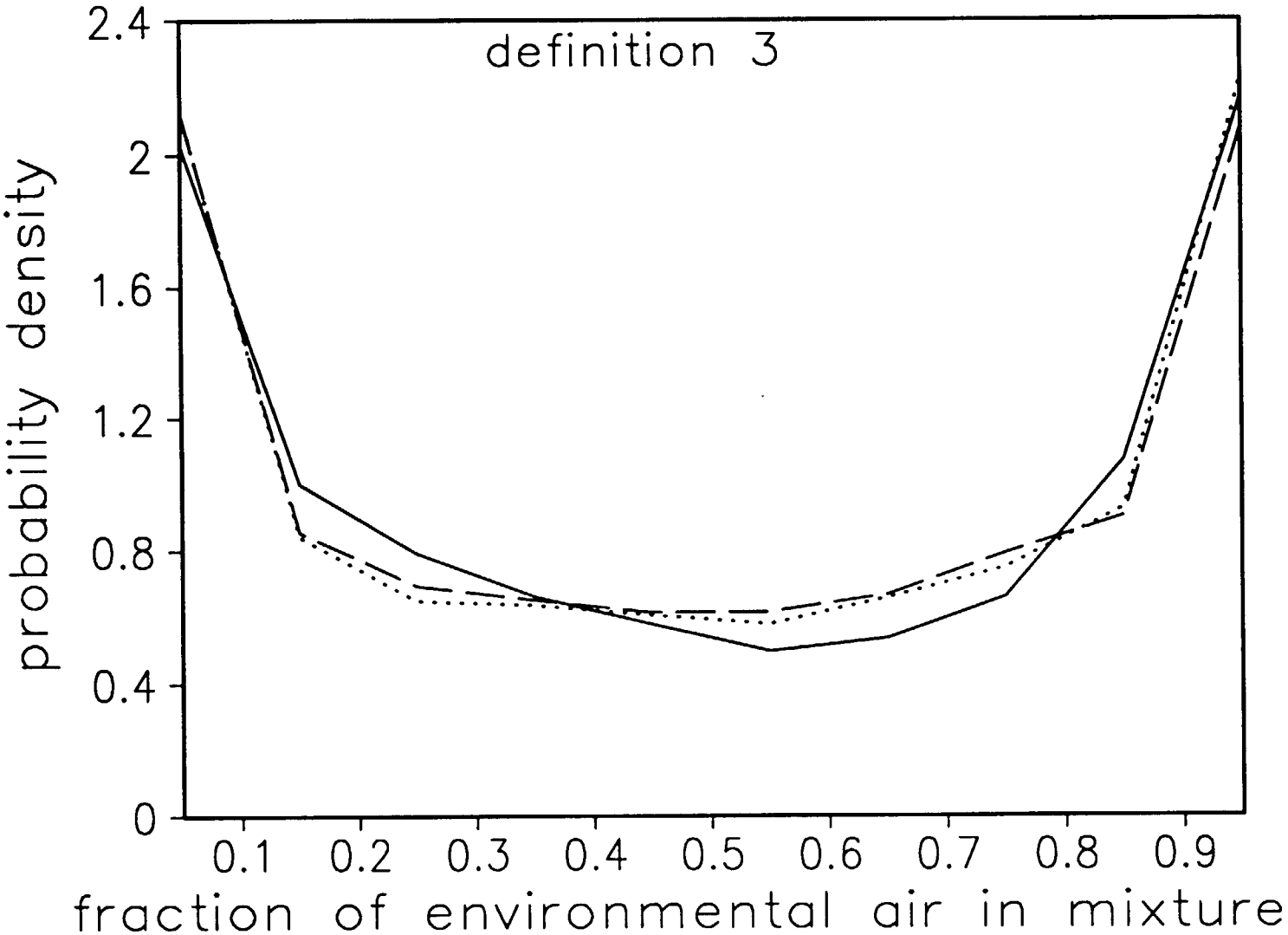

Fig. 3: Distribution of mixing fractions for definition 3 using intervals of 100 sec. (solid), 200 sec. (dashed), and 300 sec. (dotted) between re-initializing the tracers.

GrADS: COLA/IGES

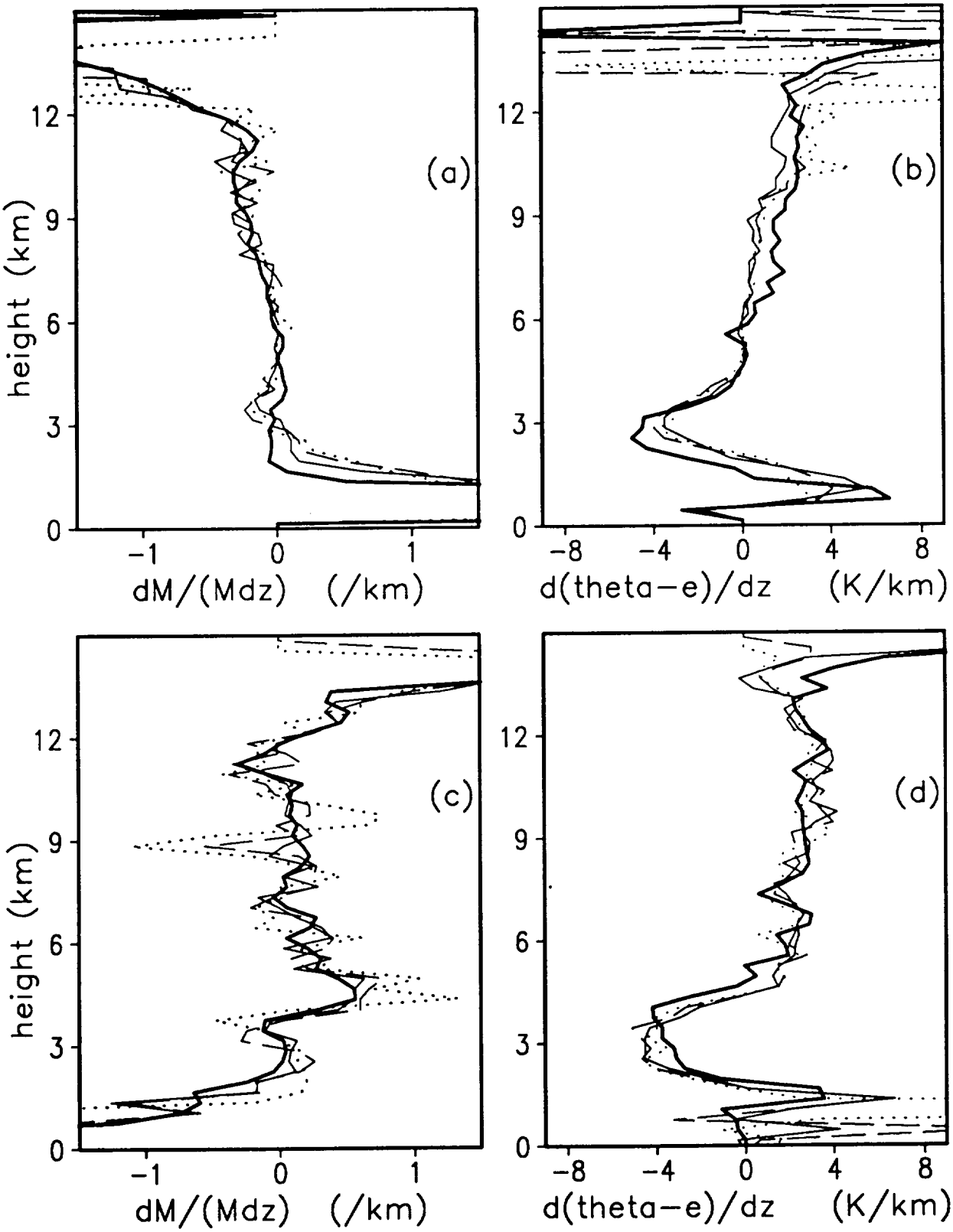

Fig. 4: Fractional change of mass flux with height for the updraft (a) and downdraft (c) and vertical gradients of equivalent potential temperature in the updraft (b) and downdraft (d), using definition 3. The heavy solid lines show the actual values in the simulation; the thin lines show the values computed from the quantities diagnosed with the tracers, using intervals of 100 sec. (solid), 200 sec. (dashed), and 300 sec. (dotted).

GrADS: COLA/IGES

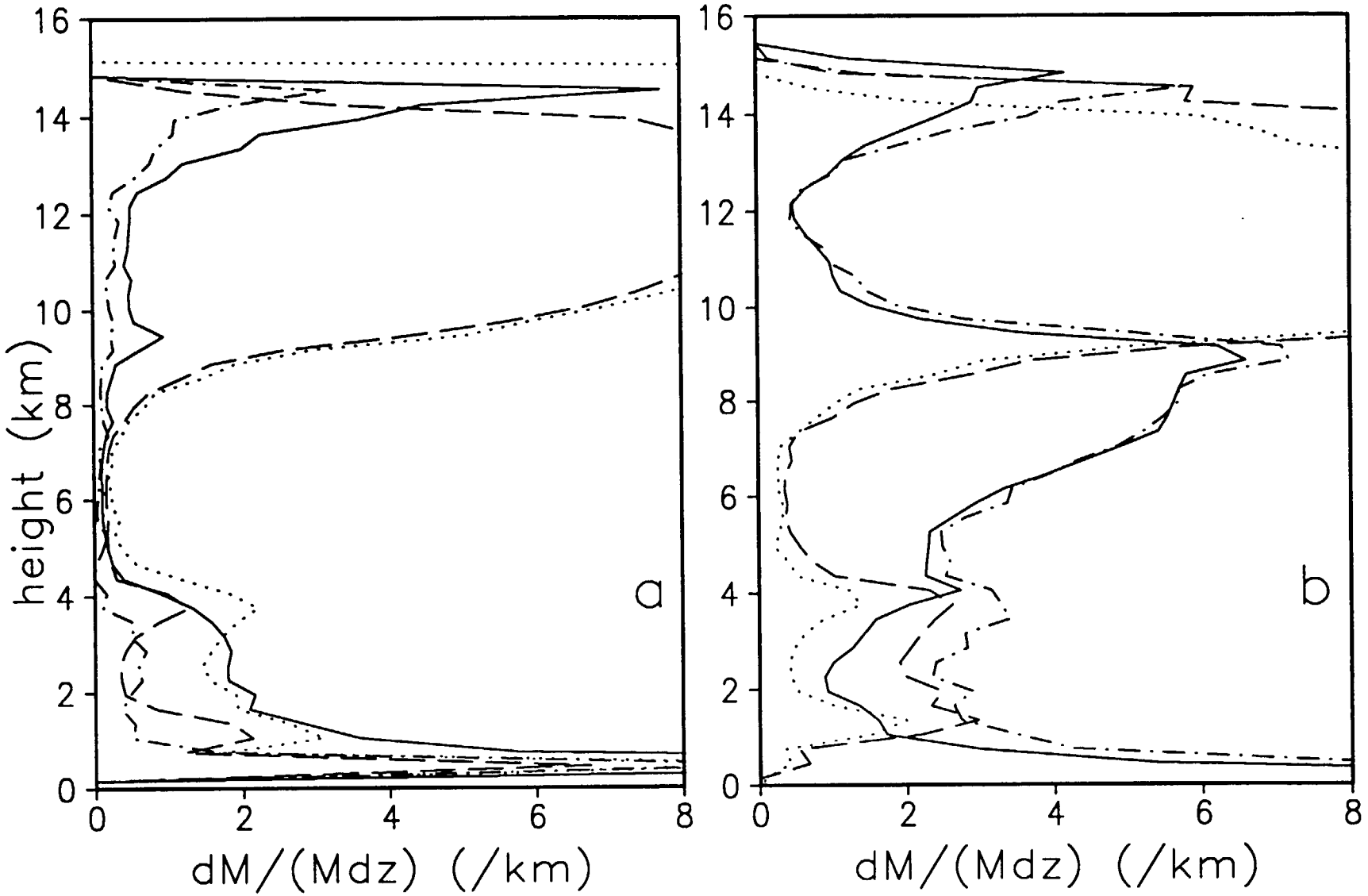

Fig. 5: Fractional entrainment and detrainment rates using definition 1: (a) entrainment of environmental air (solid) and downdraft air (dashed) into the updraft; detrainment of updraft air to the environment (dot–dash) and to the downdraft (dotted); (b) entrainment of environmental air (solid) and updraft air (dashed) into the downdraft; detrainment of downdraft air to the environment (dot–dash) and to the updraft (dotted).

GrADS: COLA/IGES

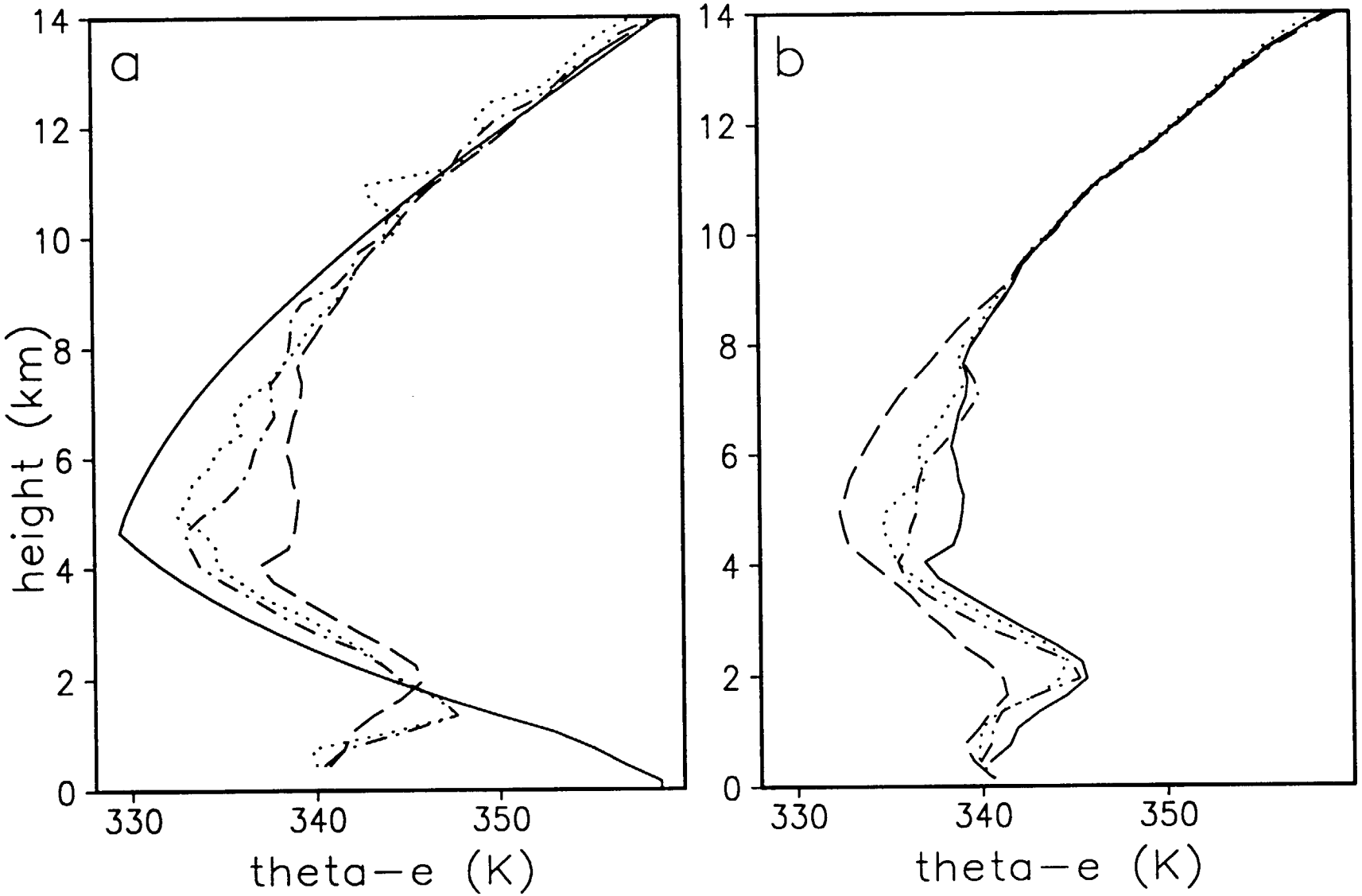

Fig. 6: Equivalent potential temperature: (a) undisturbed initial sounding (solid), updraft (dashed), and, using definition 1, entrained by the updraft from the environment (dot–dash) and detrained by the updraft to the environment (dotted); (b) updraft (solid), downdraft (dashed), and, using definition 1, transferred from updraft to downdraft (dotted) and transferred from downdraft to updraft (dot–dash).

GrADS: COLA/IGES

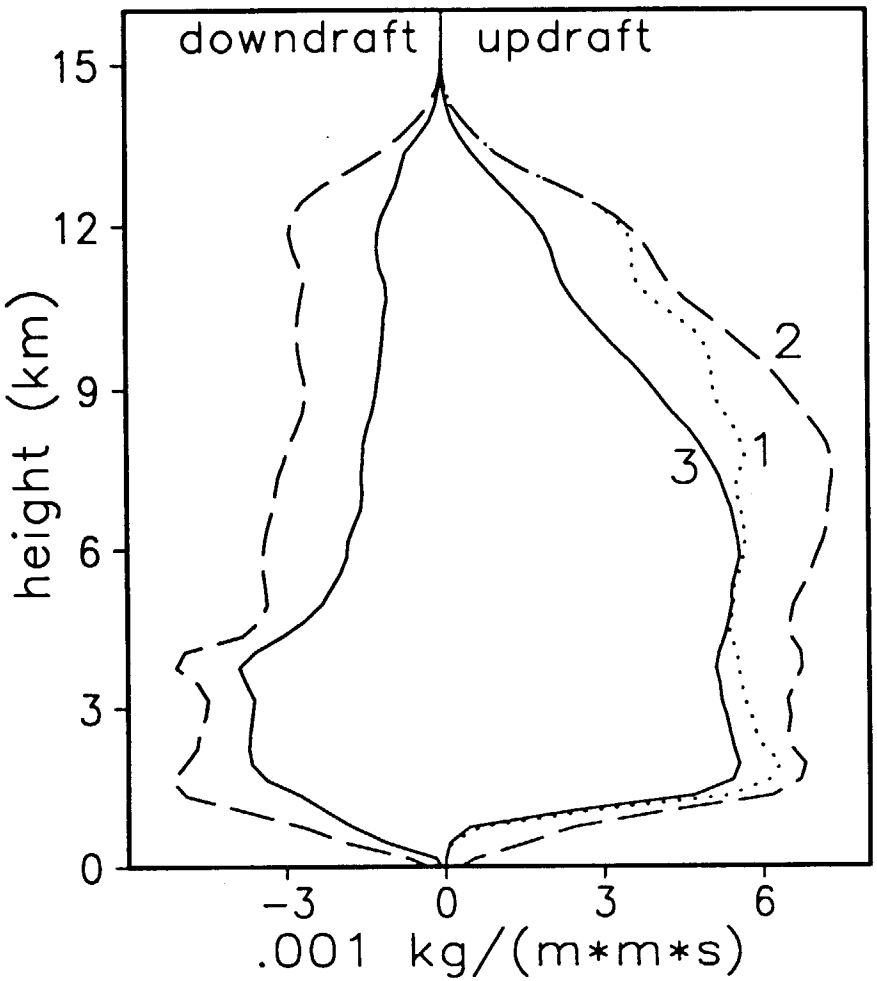

Fig. 7 Horizontally averaged, time–averaged cloud mass flux using definition 1 (dotted), definition 2 (dashed), and definition 3 (solid). Updraft mass fluxes are shown by the positive curves; downdraft mass fluxes are shown by the negative curves. Downdraft mass fluxes are identical for the first two definitions.

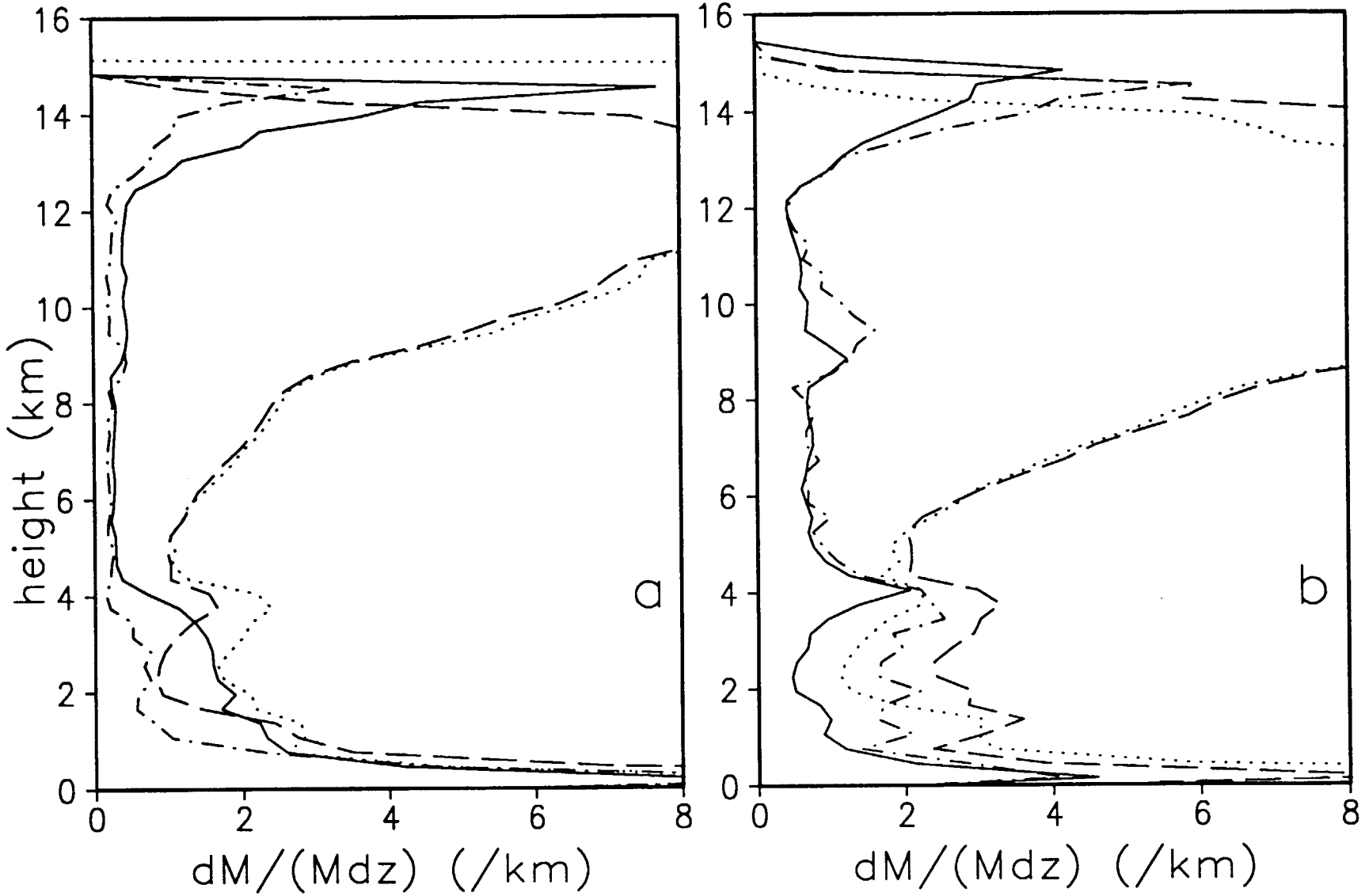

Fig. 8: Fractional entrainment and detrainment rates using definition 2: (a) entrainment of environmental air (solid) and downdraft air (dashed) into the updraft; detrainment of updraft air to the environment (dot–dash) and to the downdraft (dotted); (b) entrainment of environmental air (solid) and updraft air (dashed) into the downdraft; detrainment of downdraft air to the environment (dot–dash) and to the updraft (dotted).

GrADS: COLA/IGES

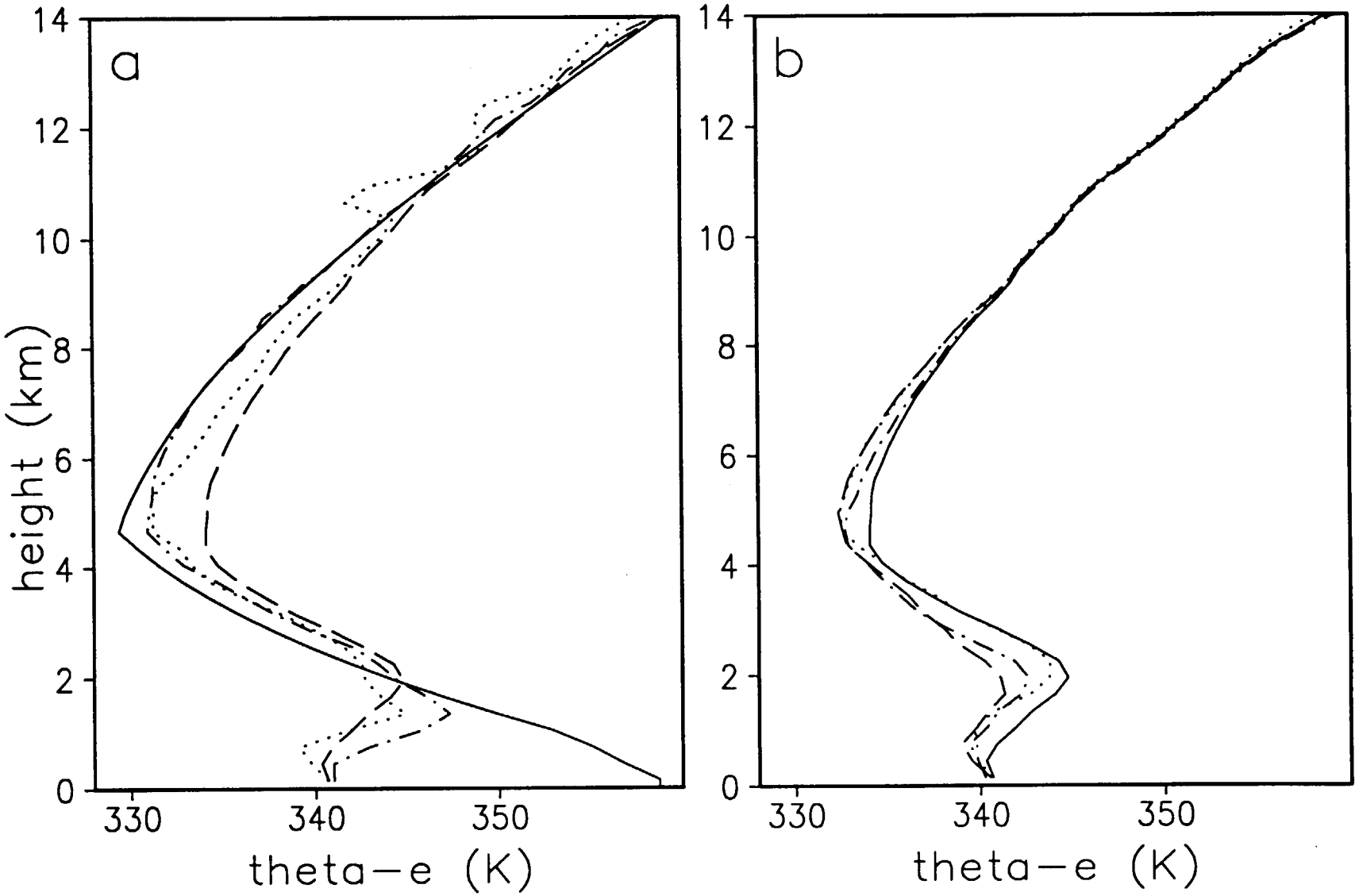

Fig. 9: Equivalent potential temperature: (a) undisturbed initial sounding (solid), updraft (dashed), and, using definition 2, entrained by the updraft from the environment (dot−dash) and detrained by the updraft to the environment (dotted); (b) updraft (solid), downdraft (dashed), and, using definition 2, transferred from updraft to downdraft (dotted) and transferred from downdraft to updraft (dot−dash).

GrADS: COLA/IGES

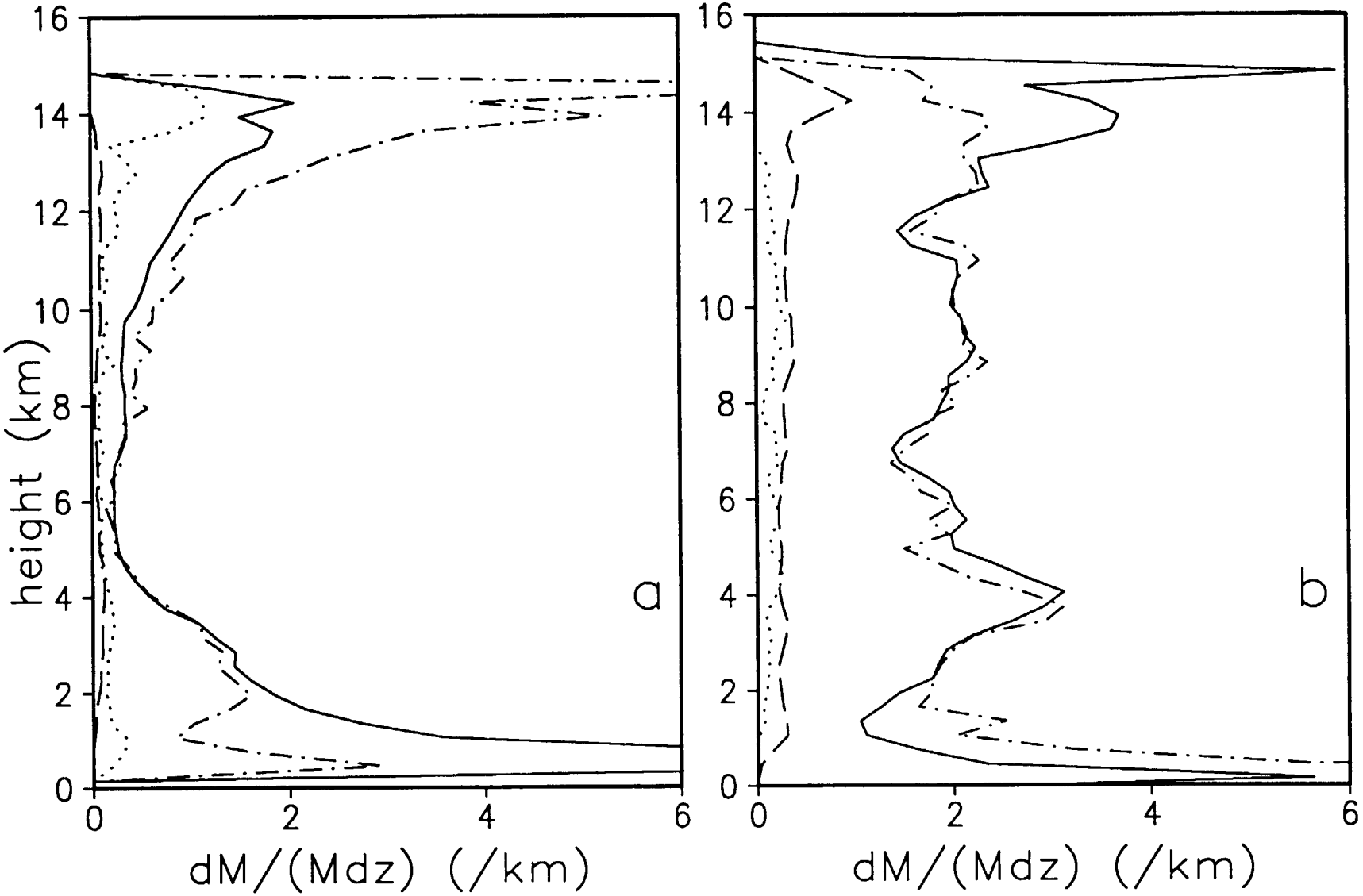

Fig. 10: Fractional entrainment and detrainment rates using definition 3: (a) entrainment of environmental air (solid) and downdraft air (dashed) into the updraft; detrainment of updraft air to the environment (dot–dash) and to the downdraft (dotted); (b) entrainment of environmental air (solid) and updraft air (dashed) into the downdraft; detrainment of downdraft air to the environment (dot–dash) and to the updraft (dotted).

GrADS: COLA/IGES

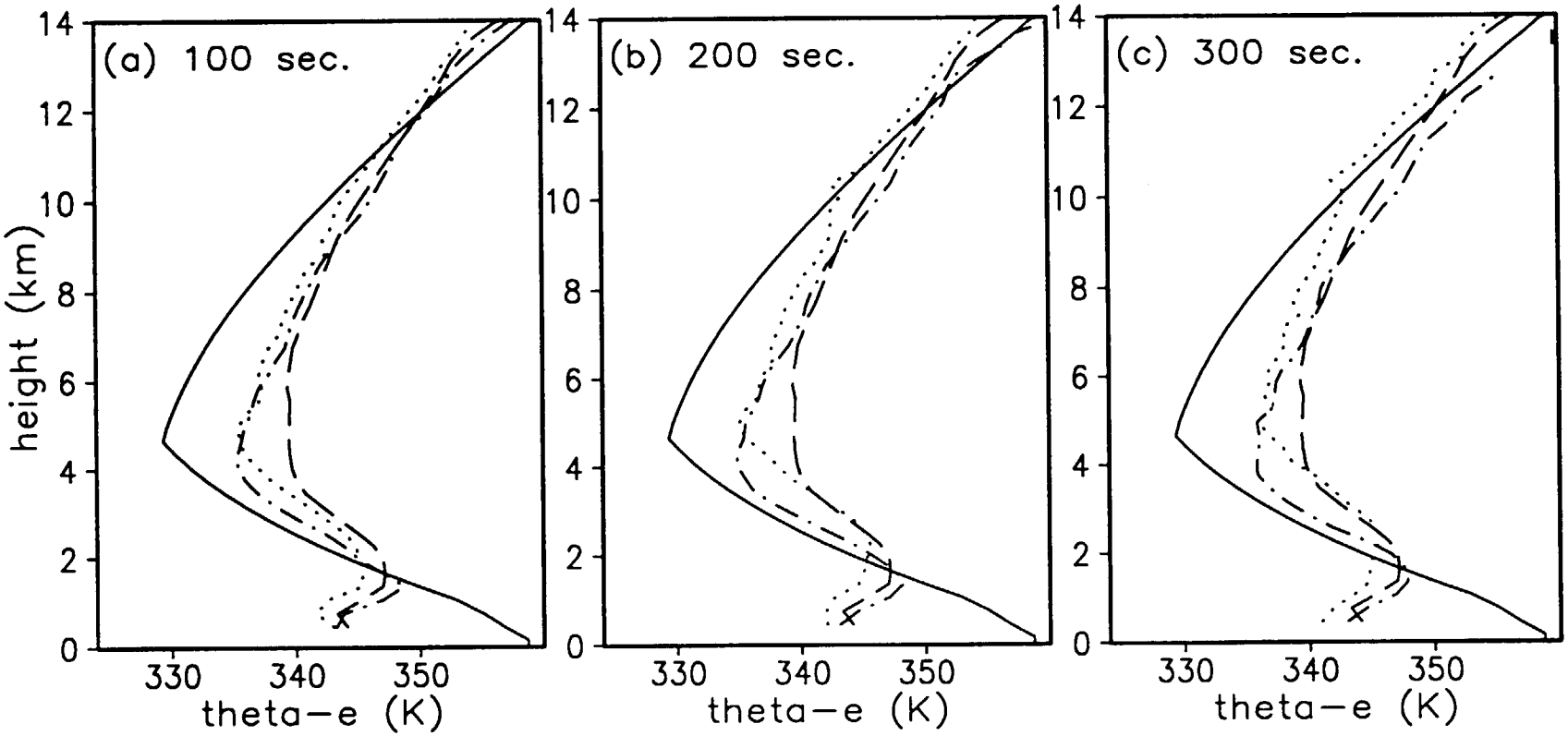

Fig. 11: Equivalent potential temperature: undisturbed initial sounding (solid), updraft (dashed), and, for definition 3, entrained by the updraft (dot−dash) and detrained by the updraft (dotted), using intervals of (a) 100 sec., (b) 200 sec., and (c) 300 sec. between re−initializing the tracers.

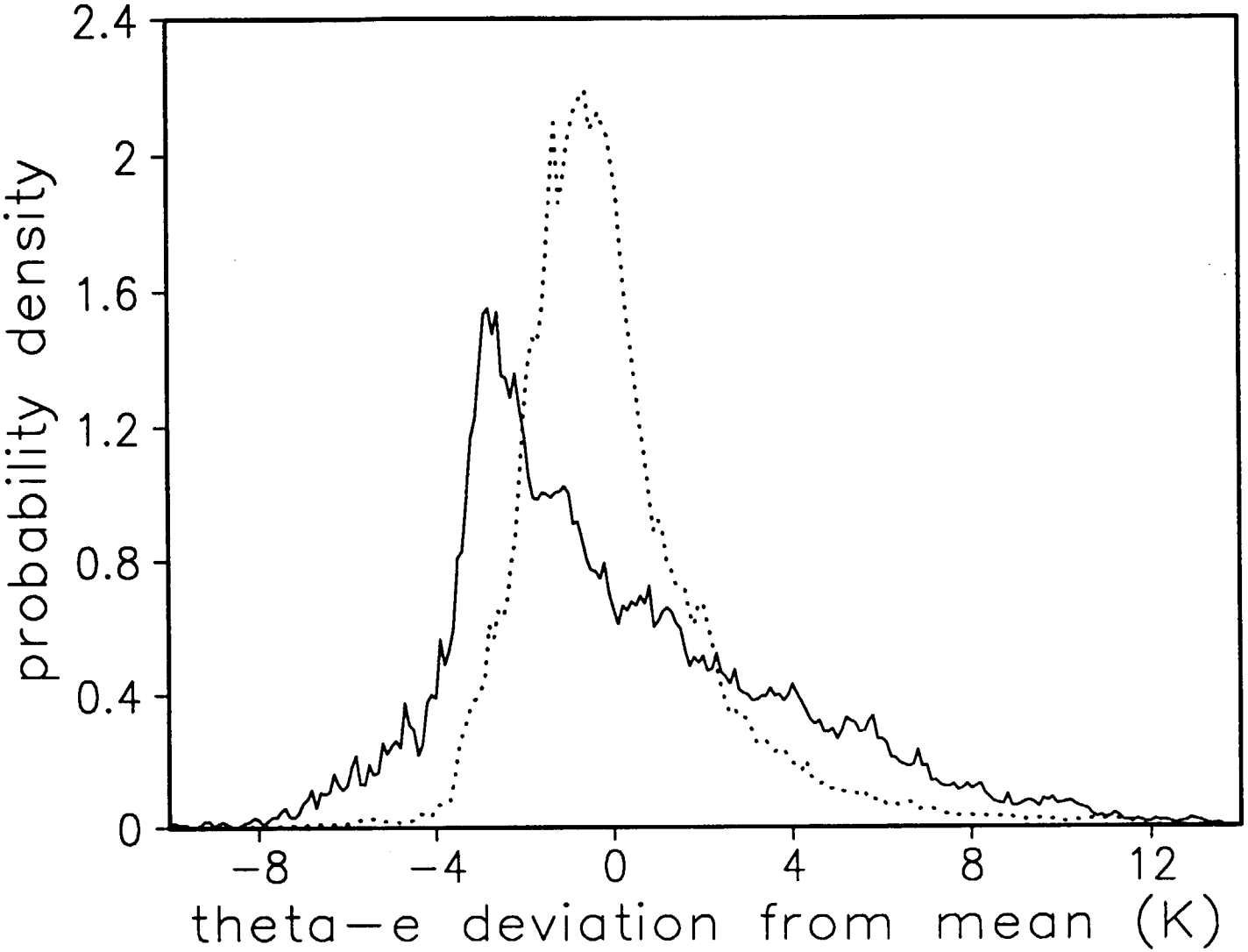

Fig. 12: Probability density function of deviations of updraft equivalent potential temperature from its mean value for updrafts at the same level, using definition 3, for all grid points below (solid) and above (dashed) 6.9 km.

GrADS: COLA/IGES

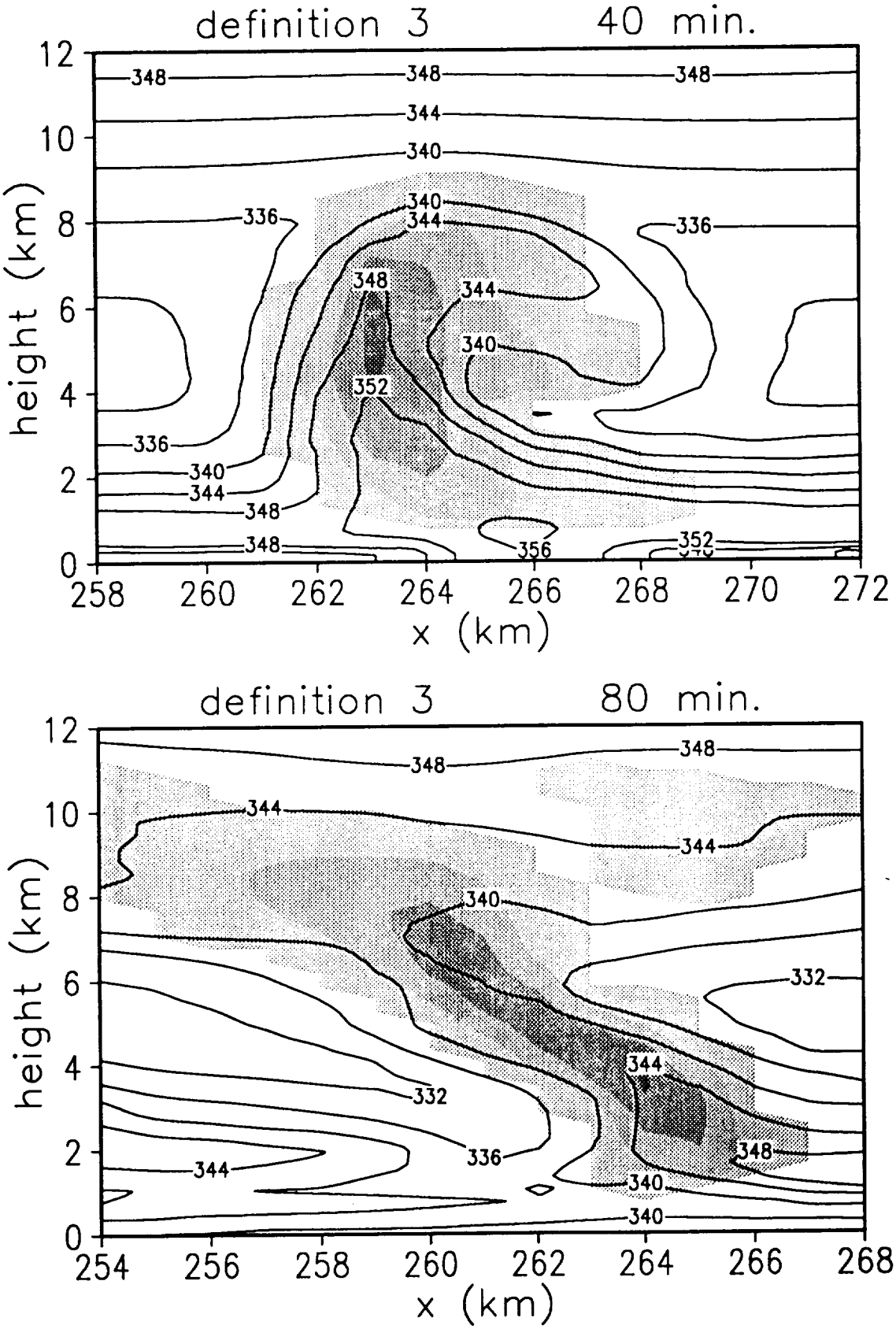

Fig. 13: Instantaneous fields at 40 min. (top) and 80 min. (bottom) of equivalent potential temperature (solid contours, with 4 K interval) and updraft mass flux (using definition 3; shading). Updraft mass fluxes are shown with intervals of 5 kg/(m*m*s) (top) and 2 kg/(m*m*s) (bottom).

GrADS: COLA/IGES

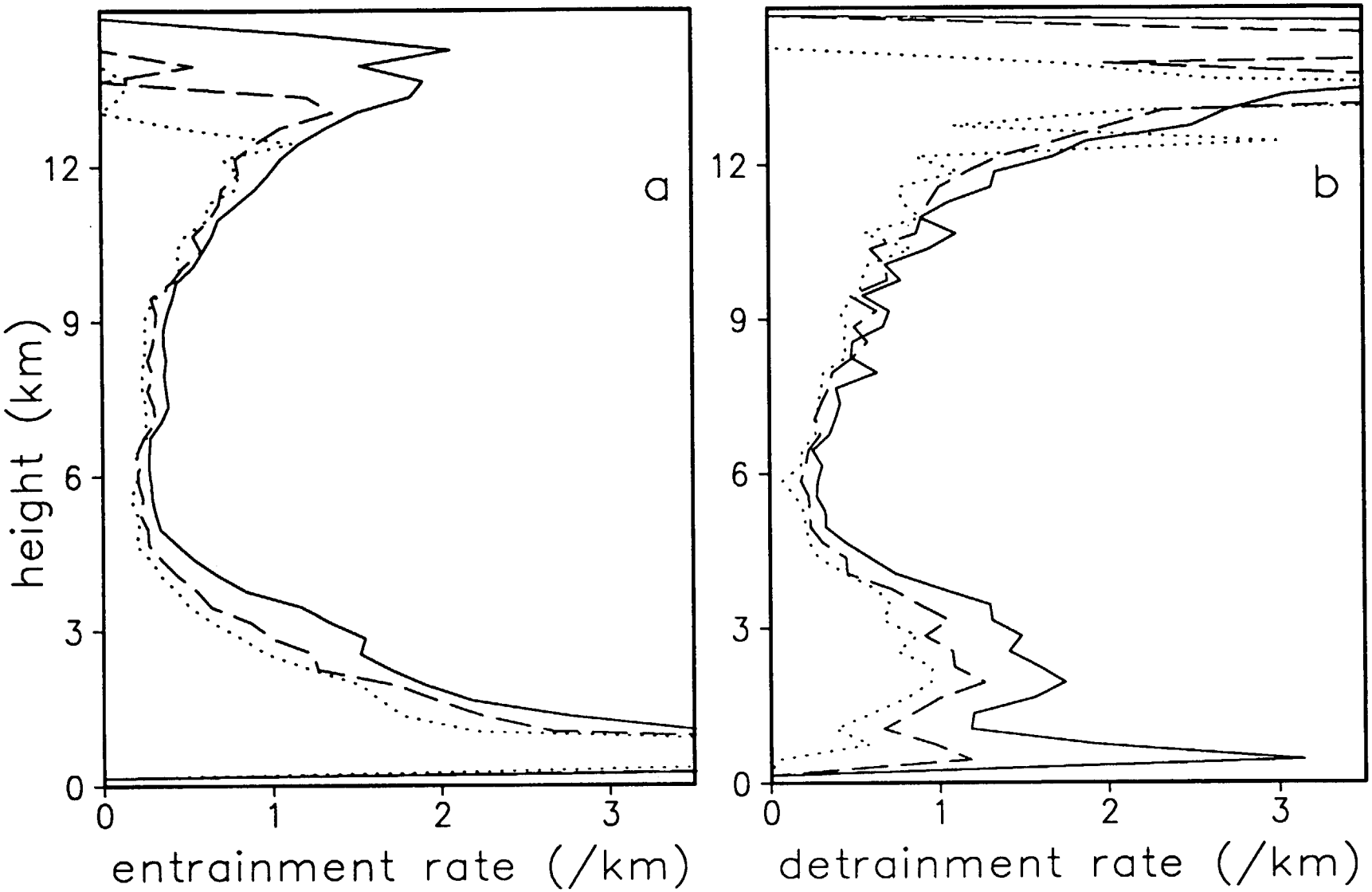

Fig. 14: Fractional entrainment rates (a) and fractional detrainment rates (b) for definition 3, using intervals of (a) 100 sec., (b) 200 sec., and (c) 300 sec. between re-initializing the tracers.

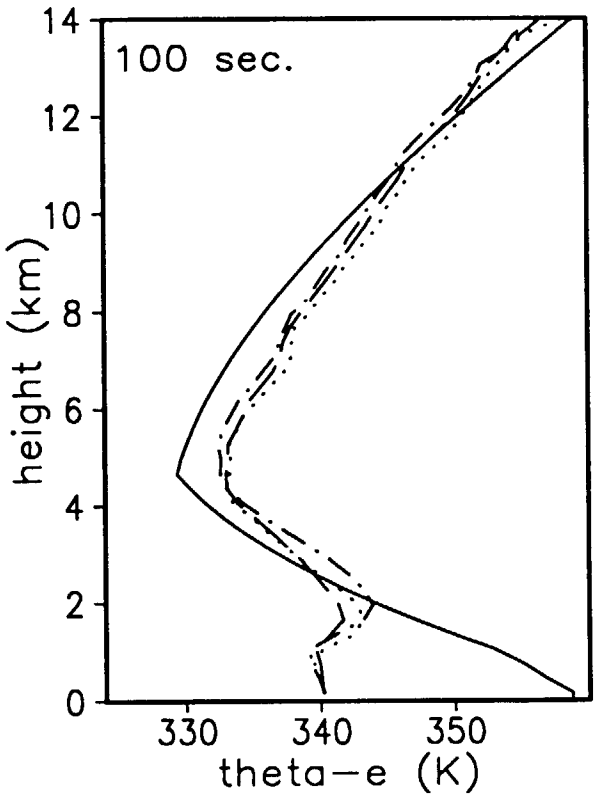

Fig. 15: Equivalent potential temperature: undisturbed initial sounding (solid), downdraft (dashed) and for definition 3, entrained by the downdraft (dot–dash) and detrained by the downdraft (dotted), using an interval of 100 sec. between re–initializing the tracers.